



Düzce University Journal of Science & Technology

Research Article

3D Electromagnetic Analysis and Optimization of Metamaterial Constructed by SRR Using the MOGA Algorithm for Performance Improvement

 Ismail TOPALOĞLU^{a,*}

^a Department of Electric Electronic Engineering, Faculty of Engineering, Cankiri Karatekin University, Cankiri, TURKEY

* Corresponding author's e-mail address: itopaloglu@karatekin.edu.tr

DOI: 10.29130/dubited.885029

ABSTRACT

The study presents 3D electromagnetic analysis and optimization of metamaterial constructed split ring resonator. The analysis was carried out under electromagnetic analysis conditions by using electromagnetic boundary conditions master and slave. The operating frequency range, in other words the performance characteristic, has been analysed from 1 GHz to 20 GHz. The split-ring resonator design has been analysed on triple co-axes in accordance with its actual use. Surface current density, electric field strength and magnetic field strength values were examined in the analysis. Metamaterial based split-ring resonators are used in many fields. Today, it has many applications as measurement and sensor or as antenna in 5G applications. In order to obtain a suitable design at high frequencies, micron-level designs are required. Newly developed objective functions are presented in the study. In this study, good results were obtained with an optimized SRR design by using multi-objective genetic algorithm in the range up to 20 GHz that can achieve negative refractive index capacity. These results are presented in the study with the relationship between permittivity and permeability. Furthermore, when the results obtained from the design are examined, it is seen that it is suitable for wireless applications. Performance improvement have been carried out SRR negative refractive index capacity which before has 11 GHz was increased to 15.5 GHz.

Keywords: Resonator, Electromagnetic, Optimization, MOGA, SRR.

Meta-malzeme Yapılı Ayrık Halka Rezonatörün Performans İyileştirmesi için MOGA Algoritması Kullanılarak Üç Boyutlu Elektromanyetik Analizi ve Optimizasyonu

ÖZET

Çalışma, meta-malzeme yapılı ayrık halka rezonatörün 3D elektromanyetik analizini ve optimizasyonunu sunar. Analiz, elektromanyetik analiz koşulları altında, ana ve bağımlı elektromanyetik sınır koşulları kullanılarak gerçekleştirilmiştir. Çalışma frekansı aralığı yani performans özelliği 1 GHz'den 20 GHz'e kadar frekans aralığında analiz edilmiştir. Ayrık halkalı rezonatör tasarımı, gerçek kullanımına uygun olarak üçlü eş eksenler üzerinde analiz edilmiştir. Analizde yüzey akım yoğunluğu, elektrik alan şiddeti ve manyetik alan şiddeti değerleri incelenmiştir. Meta-malzeme yapılı ayrık halka rezonatörler birçok alanda kullanılmaktadır. Günümüzde 5G uygulamalarında ölçüm ve sensör veya anten olarak birçok uygulama alanına sahiptir. Yüksek frekanslarda uygun bir tasarım elde etmek için mikron seviyesinde tasarımlara ihtiyaç vardır. Yeni geliştirilmiş amaç fonksiyonları çalışmada sunulmuştur. Bu çalışmada, negatif kırılma indisi kapasitesine ulaşabilen 20 GHz'e kadar çok amaçlı genetik algoritma kullanılarak optimize edilmiş bir SRR tasarımı ile iyi sonuçlar elde edilmiştir. Bu sonuçlar, çalışmada geçirgenlik ve geçirgenlik arasındaki ilişki ile sunulmuştur. Ayrıca tasarımdan elde edilen sonuçlar

incelendiğinde kablosuz uygulamalara uygun olduğu görülmektedir. Daha önce 11 GHz olan SRR negatif kırılma indisi kapasitesi performans iyileştirmesi ile 15.5 GHz'e çıkarılmıştır.

Anahtar Kelimeler: Rezonatör, Elektromanyetik, Optimizasyon, MOGA, SRR.

I. INTRODUCTION

Recently, split-ring resonators have been used in many fields from healthcare to materials science, from antenna to sensor [1]. Its wide use has increased the interest in split-ring resonators. The fact that its geometric shapes can be changed which is one of its biggest advantages [2-3]. Metamaterial, an artificially structured substance with exceptional electromagnetic characteristics that are not, or are not readily, accessible in nature [4]. Since the early 2000s, metamaterials in physics, electrical engineering, materials research, optics and nanoscience have grown into a fast-growing interdisciplinary field [5].

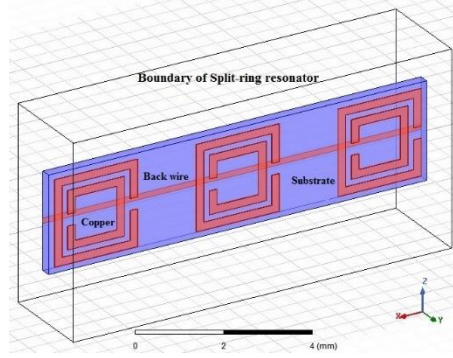


Figure 1. Split-ring resonator model

The properties of metamaterials are suited to their internal physical configuration by controlling them. This varies strikingly from natural materials, whose properties are determined primarily by their chemical elements and their interactions [6-7]. Metamaterial consists of artificial objects that are regularly or randomly spaced out that are much smaller in scale and spacing than the wavelengths of electromagnetic input [8]. As a consequence, the wave cannot overcome the microscopic information of these internal structures. For instance, it is hard to see the features of metamaterials which work with visible light at optical wavelengths and electromagnetic radiation of a shorter wavelength, such as an X-ray, for image and scan. Researcher can estimate the assembly and description of their efficient material properties on a macroscopically basis of inhomogeneous individual structures as a continuous product [9-11]. The two main parameters which qualify the electromagnetic characteristics environment are electrical permittivity (ϵ) and magnetic permeability (μ) [12]. Both parameters can be changed and now commonly used structures such as metallic wire arrays and Split-Ring Resonators (SRRs) [13]. The electric permittivity (measurement of the tendency of the electric charge within the material to decrease in electric field) can be “adjusted” to the desired value by changing the width and size of elements within metal wire arrays [14]. SRRs consist of one or two rings or squares which have a gap through which the magnetic permeability of a material can be created [15]. If an SRR is put in an external magnetic field which oscillates in the resonance frequency of the SRR, electrical current flows around the coil, which causes a small magnetic effect called a dipole magnetic moment [16-19]. With the outward oscillating field the induced dipole moment in the satellite radiography may be calibrated for a positive or negative magnetic permeability either in or out step. Thus, even though the metal used to create the SRR is non magnet, an artificial magnetism can be obtained [20-22]. Analysing such small size electromagnetic devices and sensors in two dimensions is not preferred. Very small electric field generation or surface current density on small surfaces can cause undesirable phenomena in high frequency applications. For this, making a real three-dimensional design that includes all small surfaces in the calculation will provide realistic results in the analysis. It is expected that the dimensions of the electromagnetic device pre-designed for this analysis will be simulated in all details in the analysis model. In this way, it will

be possible to obtain more precise results by establishing a detailed mesh for the regions to be analysed. The SRR model used in this study is in micron dimensions.

In response to an electromagnetic oscillating field, SRR could create an effect of being electrically smaller. The synthesis of the left hand and negative index media are used when the importance of the negative productive permeability due to the existence of the SRRs is required. When an assortment of electro-small SRRs is excited through a changing duration of magnetic field, the arrangement serves as an effective medium in a narrow band over SRR resonance [23]. The first proof of a negative refraction index was regularly assigned to the collection of SRR [24]. This proof was based on square shaped Split ring resonators in the form of a periodical, mounted cell arrangement with lined wire configuration [25]. There are various types of split-ring resonators, especially the negative refractive index. On other hand, most of the SRRs have a gap [26-27]. That is to say, each ring has a gap in its dual-ring configuration [28]. The 1-D Split Ring Structure has two square triangles, one inside [29]. The arrangement of the symmetrical ring is distinct. The structure of the Omega has a ring-structure, as the nomenclature explains [30]. The pairing form “S” was another modern metamaterial [31-35].

In this study, three-dimensional model of SRR, which was pre-designed by numerical calculation, was created with Ansoft HFSS program and boundary conditions were determined under electrostatic analysis conditions. The model created to be close to its real application that is not from a single SRR, but with triple placement and back conductor similar to the real life application and simulated for analysis. Objective functions were developed by using analysed parameters and SRR geometric dimension parameters to improve the performance of the analysed model. Performance improvement has been achieved with the multi-objective genetic algorithm (MOGA). Results from FEA, optimization results and other detailed evaluations are discussed in detail in the results section. The algorithm used for optimization includes a genetic evolutionary calculation method. Optimization of such a detailed and three-dimensional model with many parameters; it only takes weeks to prepare the simulation model. The solution to the problem takes months. Although the information processing speed of computers increases, the data and dimensions of the models simulated and analysed are also increasing at the same rate. The design values, boundary conditions, excitation areas and other details of the analysis were explained in detail in the study. It can be seen in Figure 1 designed SRR model.

II. THREE DIMENSIONAL ANALYSIS OF SPLIT-RING RESONATOR

A. DESIGN OF SPLIT-RING RESONATOR

It is necessary to create a model that includes all the details of the model to be electromagnetic analysis. Material selection should be made for the design whose model is created. It is necessary to know all the electrical and electromagnetic values of the selected material in terms of compliance with the real model. The design information of designed SRR in this study is presented in the study. Figure 2 shows the SRR geometric parameters of the designed model.

The split-ring resonator design varies according to the area where it will be used, health, antenna, and sensor as well as measuring and emitting. But basically they are designed on the basis of this situation as they operate at the point where the resonance frequency is captured. The model of SRR designed in this study is shown in Figure 2.

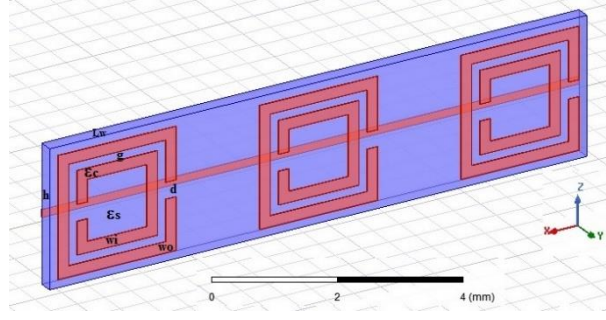


Figure 2. Geometric parameters of designed SRR

In Figure 2, h is height of substrate, g is gap between rings, L_w is substrate width, w_i is width of inner ring, w_o is width of outer ring, d is width of slit in ring, ϵ_s is permittivity of substrate material and ϵ_c is permittivity of ring material respectively. Table 1 presents initial design parameters of designed SRR.

$$L_1 = (4 * w_o) - d - (4 * w_i) \quad (1)$$

$$L_2 = (4 * w_i) - d - (4 * w_o) \quad (2)$$

$$f_1 = \frac{c}{2L_1\sqrt{\epsilon_{ff}}} , \quad f_2 = \frac{c}{2L_2\sqrt{\epsilon_{ff}}} \quad (3)$$

Eq.1, Eq.2 and Eq.3 presents sizing equations of SRR. L_1 and L_2 are inductances of outer and inner split ring resonator, respectively. C is capacitance of SRR. f_1 and f_2 are resonant frequency of SRR. Copper conductivity value is 5.96×10^7 S/m at 20 C°. The loss tangent value ranged from 0.01 to 0.035 in the 5 GHz to 20 GHz frequency band.

Table 1. Initial design parameters of SRR

Parameters	Initial value	Unit
h height of substrate	250	μm
g gap between rings	15	μm
L_w substrate width	50	μm
d width of slit in ring	35	μm
w_i width of inner ring	11.75	μm
w_o width of outer ring	22.75	μm
ϵ_s permittivity of substrate material	4.4	F/m
ϵ_c permittivity of ring material	1	F/m

B. BOUNDARY CONDITIONS FOR DESIGN

The correct determination of the boundary conditions is vital for the correct analysis of the three dimensional simulation model. It can be seen in Figure 3 master and slave boundary conditions of designed SRR which are y-z master-slave boundary and x-z master-slave boundary respectively. Master and slave boundary empower to demonstrate planes of periodicity where the E-field at each point on the slave boundary surface is compelled to coordinate the E-field of each relating point on the master limit surface. The change used to plan the E-field from the expert to the slave is controlled by determining an arrange framework on both the expert and slave limits. Both master and slave boundary consist of two main vectors U and V . In this study there are two master and two slave boundaries in the purposed model.

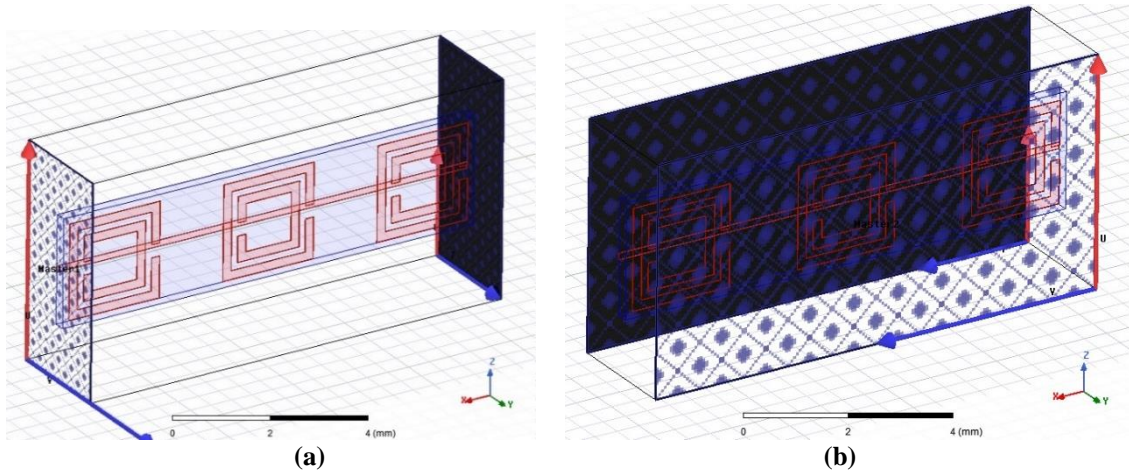


Figure 3. Master and Slave boundary conditions of designed SRR **a)** y-z Master-Slave boundary, **b)** x-z Master-Slave boundary.

Analysis of SRR model excitation system consist of two symmetrical direction port. These ports allow the SRR designed in the analysis to be analysed accurately under the applied magnetic field. It can be seen in Figure 4 excitation ports of designed SRR which are x-y-(z+) direction excitation port-1, and x-y-(z-) direction excitation port-2. The simulation model analysis for FEA is completed after when defined in the excitation system within the defined boundary conditions. Also on either side of a border are normally electrostatic fields of varying amplitudes and directions. Some limits have a surface charge, as well as surface currents which affect adjacent fields in both dynamic and static situations. The vector field flow from master to slave is always perpendicular to the surface for this boundary condition.

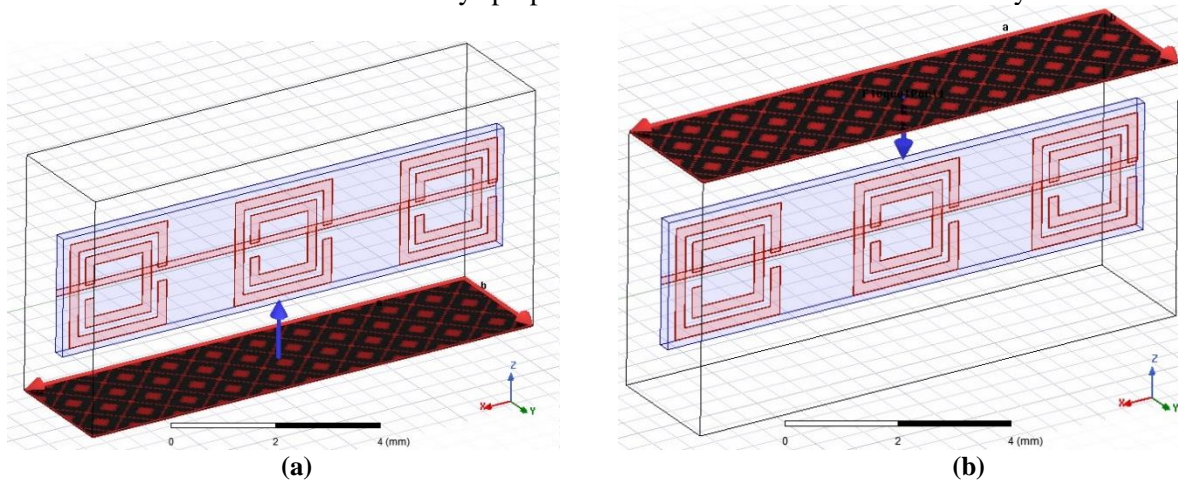


Figure 4. Excitation ports of designed SRR **a)** x-y-(z+) direction excitation port-1, **b)** x-y-(z-) direction excitation port-2.

III. ELECTROMAGNETIC ANALYSIS RESULTS

The results interpreted by the designers by adding their own experiences are important for the electromagnetic device being analysed. Three main electromagnetic parameters have been analysed which are electrical field (V/m), magnetic field intensity (A/m) and surface current density (A/m). In order to obtain FEA results, the mesh in the solution range is increased with 0.001 precision in each iteration of 15 iterations. 98765435 elements were used in total iterations. Resolution is 0.001 for this analysis and analysis takes 22 hours with 10th generation i5 processor with 6 core and 8 Gb RAM.

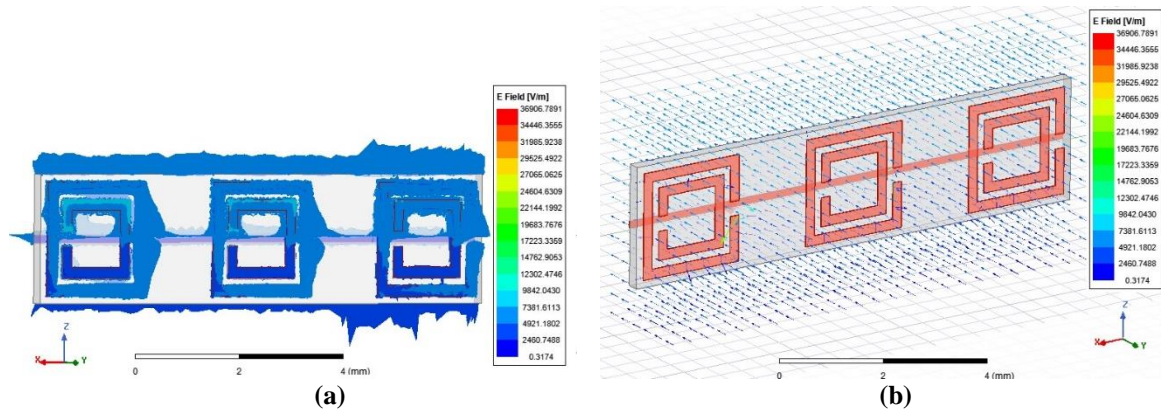


Figure 5. Electric field distribution of designed SRR **a)** E-general distribution, **b)** E-vector distribution.

When the three dimensional electrostatic analysis is made with a detailed simulation with real geometric dimension values, the results are remarkable. When the simulation results of this study are examined, it can be clearly seen in Figure 5, within the boundary conditions, the electric field is concentrated on the rings, while decreases in the dielectric substrate. Electric field vector distribution in SRR model is smooth and perpendicular the rings. It can be seen in Figure 6, within the boundary conditions, the magnetic field intensity is concentrated on the rings, while decreases in the dielectric substrate. Magnetic field intensity vector distribution in SRR model is smooth and parallel the rings. While the electric field value in the copper ring area with a large surface area is 9842 V/m, it decreases to 4921 V/m in the area where the surface area is small. It should be well understood that the amount of current passing through a cross section of the SRR is the magnetic field intensity but does not mean surface current density. The two should not be confused with each other. While the magnetic field strength acts as a vector magnitude and at the same time as a vector field, the surface current density expresses the amount of current passing through the relevant surface instantaneously. While the magnetic field intensity value is 15.91 A / m in the copper ring where the surface area is large, it decreases to 10.21 A / m in the area where the surface area is small.

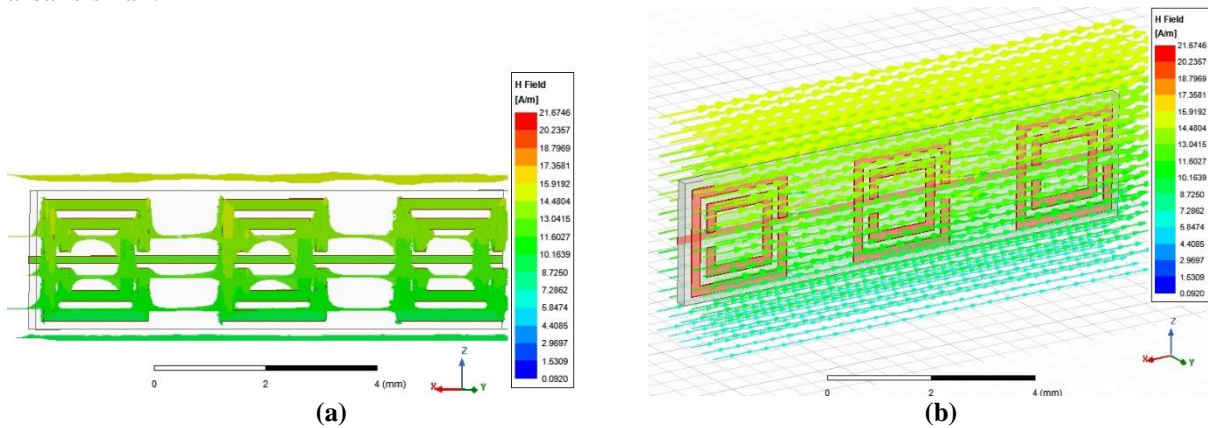


Figure 6. Magnetic field intensity distribution of designed SRR **a)** H-general distribution, **b)** H- vector distribution.

When the surface current density in Figure 7 is examined in SRR rings, it is seen that there is a distribution between 13.6 and 9.63 A/m. It can be seen that the surface current density is smooth enough to form positive and negative poles and its distribution is such that it does not disrupt the operation of the SRR. If the surface current density had an uneven distribution between the SRR rings, the ring capacitance and inductance values would change and the resonance frequency would change accordingly.

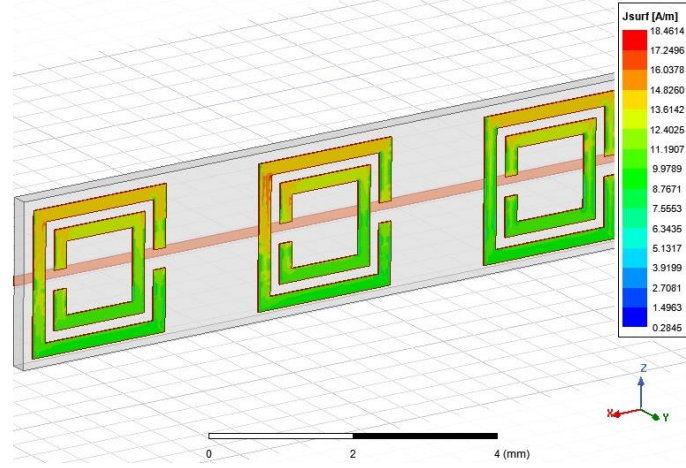


Figure 7. Surface current density distribution of designed SRR

As a result, when the results obtained with the values obtained in the electrostatic analysis are examined in depth, it can be said that the S-parameter values of SRR and the most important and difficult part of the metamaterial analysis part are also simulated correctly. All of the S-parameters of the SRR are obtained from the frequency dependent effective material parameters. In the SRR analysis, the output values were entered directly into the simulation model, which was created correctly, and the geometric relations of the model were defined.

IV. OPTIMIZATION OF SPLIT-RING RESONATOR

Optimisation is called technology/methods used to build or adjust some device/tool for the best/optimal use. The goal or purpose of optimization is to achieve a solution for a problem that is perfect, most beneficial or efficient [36-38]. This is true when dependency and limitation of the objective function (parameter to be optimized) are known to other parameters. The detection of similar parameters is therefore primarily important. Effects for objective function of these parameters are analysed, forming the basis for algorithm creation [39-42]. Under such conditions or constraints algorithms are programmed to improve (max or minimize) the objective function. In any area that needs successful solutions, optimization can be used [43-44].

Developed objective functions for SRR are shown in Eq. 4 and Eq. 5. Here, E: electric field, H: magnetic field strength, j: surface current density and f: frequency respectively. X_1 , X_2 and X_3 are status values of objective functions. Status values can be 1 or 0 depending on the type of improvement targeted. When the status values are $X_1=1$, $X_2=1$ and $X_3=1$, this means performance improvement. Objective functions take the results with results varying between 0 and 1. Results between 0 and 0.3 were defined as low correlation, between 0.3 and 0.6 as medium correlation, and between 0.6 and 1.0 as good correlation. Objective functions are used when the X parameters yielded results in a good correlation range according to their condition.

$$Of_1 = \frac{E^{x_1}}{H^{x_2} \times J^{x_3}} \quad (4)$$

$$Of_2 = \frac{E^{x_1}}{f^{x_2} \times J^{x_3}} \quad (5)$$

Multi-objective genetic algorithm scheme can be seen in Figure 8. Initially SRR selected optimization parameters population updated by genetic algorithm. Then MOGA generates new population for the optimization problem in solving area. Firstly parents used for next generation children. If the objective function constraint conditions are not met, then both the old parents and the new parents from the new population are randomly selected to generate the new generation for the new generation. If this mutation

meets the desired values, a new population is no longer produced. The values of the design parameters for optimum values are then updated according to these ideal results. Finally, the integrity of the optimum values obtained in the algorithm is checked, and if appropriate, the solution is completed, if not, the same cycle continues until the solution is found. The electromagnetic parameters selected for the objective functions developed in this study vary depending on the geometric dimension values and the frequency at the same time. Although this makes the problem much more difficult, it is the closest to a real-world simulation. In MOGA, more than one objective function can be defined independently or interdependently. This is the difference from other optimization methods. The solution is found by a genetic algorithm-based search, but multiple objective functions are used instead of a single objective function. This algorithm allows the above described to be done. That's why it was chosen.

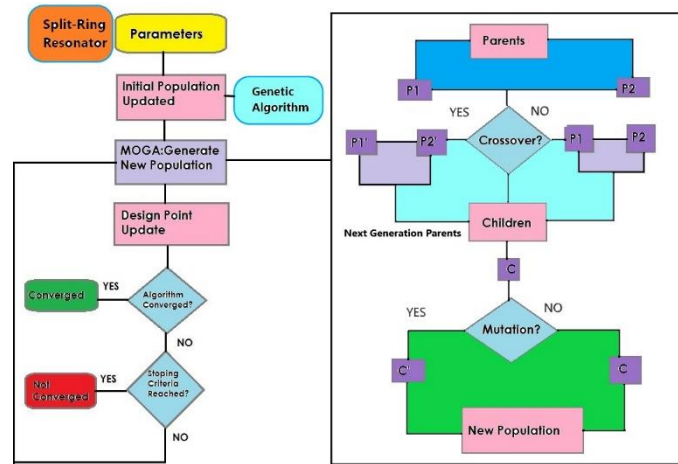
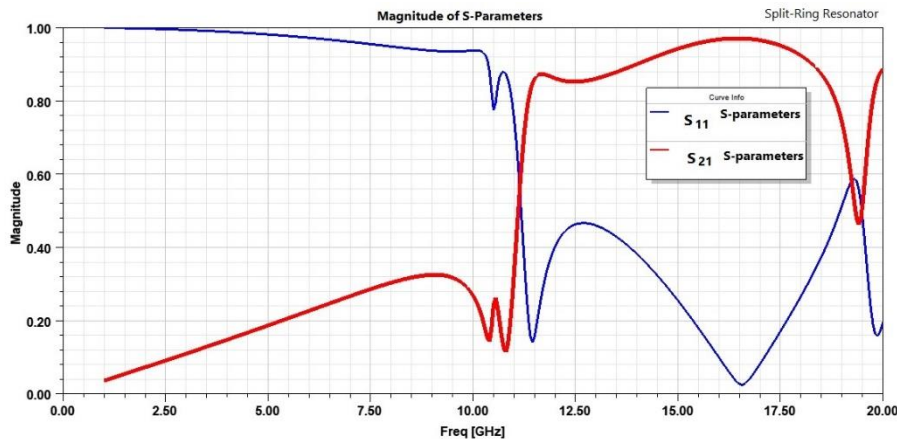


Figure 8. Multi-objective genetic algorithm scheme

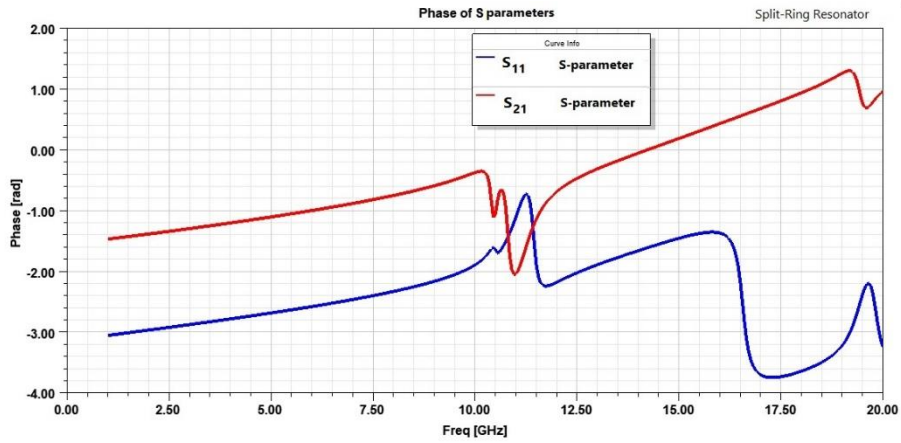
Table 2. Optimization variables and solving area

Input variable	Initial design value	MOGA search points
f , Frequency	1 GHz	1 GHz < up to < 20 GHz
L_w substrate width	50 μm	50 μm < up to < 80 μm
w_i width of inner ring	11.75 μm	11.75 μm < up to < 22.75 μm
w_o width of outer ring	22.75 μm	22.75 μm < up to < 35.175 μm

Optimization variables and optimization problem solving area values presented in Table 2. f Frequency, L_w substrate width, w_i width of inner ring and w_o width of outer ring are selected for the optimization variable. Because these selected parameters directly affect SRR performance. The initial values and solution ranges are shown in Table 2.



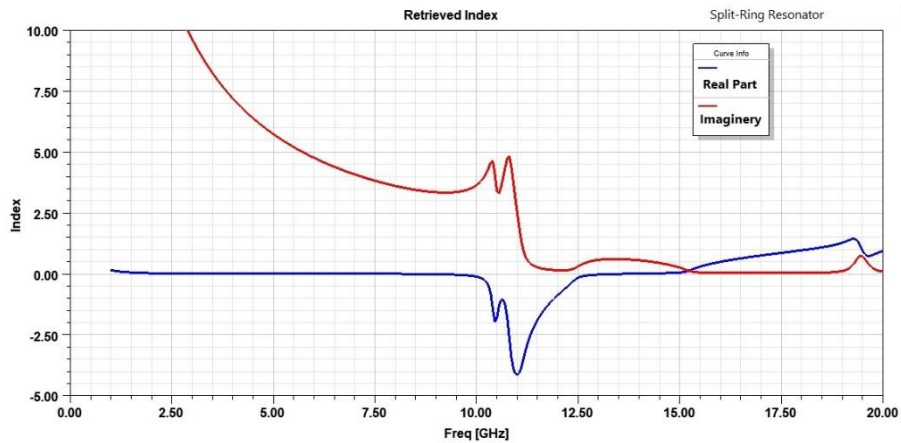
(a)



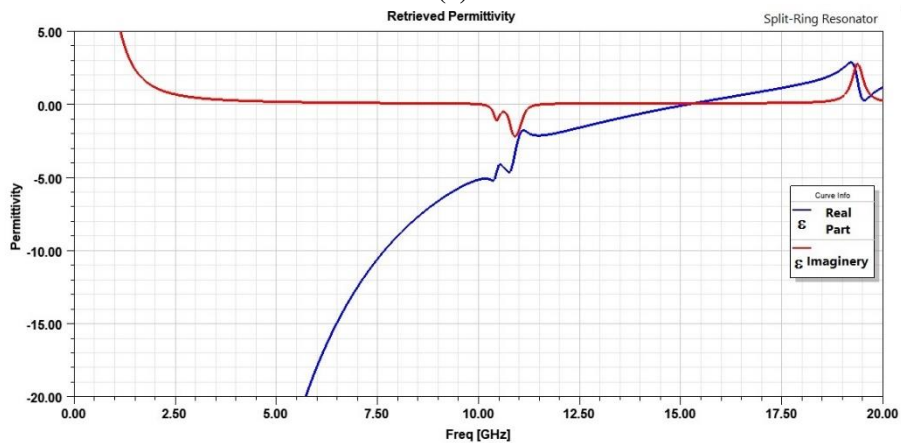
(b)

Figure 9. SRR S-parameters a) Magnitude of S-parameters, b) Phase of S-parameters.

S_{11} and S_{21} are S-parameters of designed SRR which are analysed in the study. It can be seen in Figure 9 SRR S-parameters. In Figure 9 a, magnitude of S_{11} and S_{21} with varying frequency from 1 GHz to 20 GHz. S_{11} and S_{21} parameter values intersect in the range between 11.5 GHz and 12 GHz. Phase of S_{11} and S_{21} can be seen in Figure 9 b.



(a)



(b)

Figure 10. SRR retrieved values a) refractive index, b) effective permittivity.

It can be seen in Figure 10 a, refractive index of designed SRR. This figure clearly showed that designed SRR normally produce negative refractive index characteristic to 15.5 GHz. The same situation can be seen in the other Figure 10 b, the effective permittivity value produces negative refractive index characteristic to 15.5 GHz. This is also an indication that this design, which can normally run up to 11 GHz, has been optimized to increase the operating range to 15.5 GHz. The metamaterial designed SRR analysed in this way has produced values suitable for design and optimization purposes.

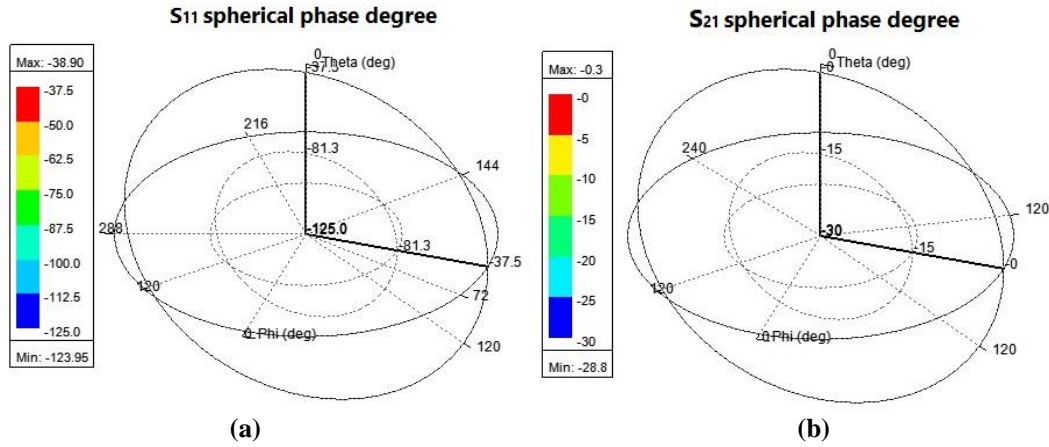


Figure 11. SRR S-parameters sphere phase degree **a)** S_{11} sphere phase, **b)** S_{21} sphere phase degree.

Designed SRR sphere phase degrees shown in Figure 11. S_{11} sphere phase degree in figure “a” and “b” for S_{21} sphere phase degree. The limits of the spherical phase degrees for each S-parameter are clearly visible. The optimization problem defined in Table 2 and the solution of the optimization problem for the solution intervals are presented in Table 3. In the optimization problem, in this study, the aim of optimization is to improve the objective functions.

Table 3. Analysis and optimization results

Input variable	Initial value	FEA	MOGA
f, Frequency	1 GHz	10.3 GHz	11.03 GHz
L_w substrate width	50 μm	65.175 μm	55.325 μm
w_i width of inner ring	11.75 μm	17.15 μm	12.25 μm
w_o width of outer ring	22.75 μm	29.10 μm	23.20 μm

FEA results and optimization results presented in the Table 3. In reality the optimum points include not only a numerical value but a solution set. The simulations made showed that the SRR design subject to the study can be used in a wide range of applications from wireless applications to antenna applications, from health applications to advanced measurement applications. SRR negative refractive index capacity was increased by approximately 4.5 GHz with the optimization work. This value corresponds to an increase of % 41. Reflection coefficients consists of S parameters and S_{11} & S_{21} in dB $S_{11} = 20\log_{10}|E_r/E_i| = 10\log_{10}|E_r/E_i|^2$, where E_r and E_i are the reflected and incident electric fields, respectively. In general, S_{11} and S_{21} are complex quantities. However, the question asked about S_{11} & S_{21} in dB, thus, from the above analysis, negative return loss provide positive S parameters.

V. CONCLUSION

In the study, three dimensional electromagnetic analysis of SRR and optimization presented. Newly developed objective functions and their status values discussed in advanced and presented in the study. Ansoft HFSS which is commercial design and analyse software used for the analysing the purposed

system. Multi-objective genetic algorithm used for the solving the optimization problem. Effective parameters of designed SRR are investigated such as S_{11} and S_{21} . Negative refractive index capacity increased almost 4.5 GHz. Finite element analysis results presented in the study such as electric field, magnetic field intensity and surface current density which are very important for the SRRs. The simulations made showed that the SRR design subject to the study can be used in a wide range of applications from wireless applications to antenna applications, from health applications to advanced measurement applications. SRR negative refractive index capacity was increased by approximately 4.5 GHz with the optimization work.

V. REFERENCES

- [1] A. Dadgarpour, B. Zarghooni, B. S. Virdee, T. A. Denidni and A. A. Kishk, "Mutual Coupling Reduction in Dielectric Resonator Antennas Using Metasurface Shield for 60-GHz MIMO Systems," in *IEEE Antennas and Wireless Propagation Letters*, vol. 16, pp. 477-480, 2017.
- [2] C. Herrojo, F. Paredes, J. Mata-Contreras, S. Zuffanelli and F. Martín, "Multistate Multiresonator Spectral Signature Barcodes Implemented by Means of S-Shaped Split Ring Resonators (S-SRRs)," in *IEEE Transactions on Microwave Theory and Techniques*, vol. 65, no. 7, pp. 2341-2352, 2017.
- [3] P. Vélez, L. Su, K. Grenier, J. Mata-Contreras, D. Dubuc and F. Martín, "Microwave Microfluidic Sensor Based on a Microstrip Splitter/Combiner Configuration and Split Ring Resonators (SRRs) for Dielectric Characterization of Liquids," in *IEEE Sensors Journal*, vol. 17, no. 20, pp. 6589-6598, 2017.
- [4] A. Ebrahimi, J. Scott and K. Ghorbani, "Differential Sensors Using Microstrip Lines Loaded With Two Split-Ring Resonators," in *IEEE Sensors Journal*, vol. 18, no. 14, pp. 5786-5793, 2018.
- [5] M. Abdolrazzagli and M. Daneshmand, "Exploiting Sensitivity Enhancement in Micro-wave Planar Sensors Using Intermodulation Products With Phase Noise Analysis," in *IEEE Transactions on Circuits and Systems I: Regular Papers*, vol. 67, no. 12, pp. 4382-4395, 2020.
- [6] T. Haq, C. Ruan, S. Ullah and A. Kosar Fahad, "Dual Notch Microwave Sensors Based on Complementary Metamaterial Resonators," in *IEEE Access*, vol. 7, pp. 153489-153498, 2019.
- [7] B. Camli, E. Kusakci, B. Lafci, S. Salman, H. Torun and A. D. Yalcinkaya, "Cost-Effective, Microstrip Antenna Driven Ring Resonator Microwave Biosensor for Biospecific Detection of Glucose," in *IEEE Journal of Selected Topics in Quantum Electronics*, vol. 23, no. 2, pp. 404-409, Art no. 6900706, 2017.
- [8] K. Xu *et al.*, "Novel Microwave Sensors Based on Split Ring Resonators for Measuring Permittivity," in *IEEE Access*, vol. 6, pp. 26111-26120, 2018.
- [9] J. Hinojosa, M. Rossi, A. Saura-Ródenas, A. Álvarez-Melcón and F. L. Martínez-Viviente, "Compact Bandstop Half-Mode Substrate Integrated Waveguide Filter Based on a Broadside-Coupled Open Split-Ring Resonator," in *IEEE Transactions on Microwave Theory and Techniques*, vol. 66, no. 6, pp. 3001-3010, 2018.
- [10] W. Tang, G. Goussetis, N. J. G. Fonseca, H. Legay, E. Sáenz and P. de Maagt, "Coupled Split-Ring Resonator Circular Polarization Selective Surface," in *IEEE Transactions on Antennas and Propagation*, vol. 65, no. 9, pp. 4664-4675, 2017.

- [11] G. Govind, N. K. Tiwari, K. K. Agrawal and M. J. Akhtar, "Microwave Subsurface Imaging of Composite Structures Using Complementary Split Ring Resonators," in *IEEE Sensors Journal*, vol. 18, no. 18, pp. 7442-7449, 2018.
- [12] J. Mata-Contreras, C. Herrojo and F. Martín, "Application of Split Ring Resonator (SRR) Loaded Transmission Lines to the Design of Angular Displacement and Velocity Sensors for Space Applications," in *IEEE Transactions on Microwave Theory and Techniques*, vol. 65, no. 11, pp. 4450-4460, 2017.
- [13] T. Yue, Z. H. Jiang, A. H. Panaretos and D. H. Werner, "A Compact Dual-Band Antenna Enabled by a Complementary Split-Ring Resonator-Loaded Metasurface," in *IEEE Transactions on Antennas and Propagation*, vol. 65, no. 12, pp. 6878-6888, 2017.
- [14] M. A. H. Ansari, A. K. Jha, Z. Akhter and M. J. Akhtar, "Multi-Band RF Planar Sensor Using Complementary Split Ring Resonator for Testing of Dielectric Materials," in *IEEE Sensors Journal*, vol. 18, no. 16, pp. 6596-6606, 2018.
- [15] T. Athauda and N. C. Karmakar, "The Realization of Chipless RFID Resonator for Multiple Physical Parameter Sensing," in *IEEE Internet of Things Journal*, vol. 6, no. 3, pp. 5387-5396, 2019.
- [16] J. S. Bobowski and A. P. Clements, "Permittivity and Conductivity Measured Using a Novel Toroidal Split-Ring Resonator," in *IEEE Transactions on Microwave Theory and Techniques*, vol. 65, no. 6, pp. 2132-2138, 2017.
- [17] A. B. de Alleluia *et al.*, "Experimental Testing of a 3-D-Printed Metamaterial Slow Wave Structure for High-Power Microwave Generation," in *IEEE Transactions on Plasma Science*, vol. 48, no. 12, pp. 4356-4364, 2020.
- [18] R. A. Dextre, T. Yamauchi, K. A. Polzin and K. G. Xu, "Concentric Split-Ring Resonator Microwave Microplasma Generation at Off-Resonant Frequencies," in *IEEE Transactions on Plasma Science*, vol. 48, no. 4, pp. 827-834, 2020.
- [19] A. A. G. Amer, S. Z. Sapuan, N. Nasimuddin, A. Alphones and N. B. Zinal, "A Comprehensive Review of Metasurface Structures Suitable for RF Energy Harvesting," in *IEEE Access*, vol. 8, pp. 76433-76452, 2020.
- [20] X. Liu, W. Wu, P. Ji and N. Yuan, "Design of Compact Dual-Passband Filters by Parasitic Passband With Controllable Passbands," in *IEEE Microwave and Wireless Components Letters*, vol. 28, no. 5, pp. 410-412, 2018.
- [21] M. Li, X. Chen, A. Zhang, W. Fan and A. A. Kishk, "Split-Ring Resonator-Loaded Baffles for Decoupling of Dual-Polarized Base Station Array," in *IEEE Antennas and Wireless Propagation Letters*, vol. 19, no. 10, pp. 1828-1832, 2020.
- [22] S. Ma, L. Sydänheimo, L. Ukkonen and T. Björninen, "Split-Ring Resonator Antenna System With Cortical Implant and Head-Worn Parts for Effective Far-Field Implant Communications," in *IEEE Antennas and Wireless Propagation Letters*, vol. 17, no. 4, pp. 710-713, 2018.
- [23] C. Tseng and C. Wu, "A Novel Microwave Phased- and Perturbation-Injection-Locked Sensor With Self-Oscillating Complementary Split-Ring Resonator for Finger and Wrist Pulse Detection," in *IEEE Transactions on Microwave Theory and Techniques*, vol. 68, no. 5, pp. 1933-1942, 2020.
- [24] P. Vélez, J. Muñoz-Enano, K. Grenier, J. Mata-Contreras, D. Dubuc and F. Martín, "Split Ring Resonator-Based Microwave Fluidic Sensors for Electrolyte Concentration Measurements," in *IEEE Sensors Journal*, vol. 19, no. 7, pp. 2562-2569, 2019.

- [25] U. Kose and A. Kavas, "Design and Performance Analysis of Split Ring Resonator Based Microstrip Antenna With Defected Ground Structure," *2020 4th International Symposium on Multidisciplinary Studies and Innovative Technologies (ISMSIT)*, Istanbul, Turkey, 2020, pp. 1-4.
- [26] L. Wu, J. Sheng, S. Peng, Z. Xiao and S. Gu, "Chipless RFID Tag using Complementary Hexagonal Split Ring Resonator," *2019 IEEE Asia-Pacific Microwave Conference (APMC)*, Singapore, 2019, pp. 1334-1336.
- [27] X. Jiang, P. Zhong, Q. Zhang and A. K. Rashid, "A Broadband Metamaterial Polarization Converter Based on Split Ring Resonators," *2019 Cross Strait Quad-Regional Radio Science and Wireless Technology Conference (CSQRWC)*, Taiyuan, China, 2019, pp. 1-3.
- [28] B. Chowdhury, T. Walpita, B. Yang and A. Eroglu, "Resonant Characteristics of Split Ring Resonator And Unit Cell for Periodic Metamaterial Devices," *2020 International Applied Computational Electromagnetics Society Symposium (ACES)*, Monterey, CA, USA, 2020, pp. 1-2.
- [29] Y. Liu, X. Dang, L. Li and H. Yin, "Planar microwave retroreflector based on a split ring resonator metasurface," *2019 International Applied Computational Electromagnetics Society Symposium - China (ACES)*, Nanjing, China, 2019, pp. 1-2.
- [30] Y. Khanna, R. Gaur, R. Gupta and Y. K. Awasthi, "Design of Metamaterial by Slotted Split Ring Resonator-SSRR for Dual Frequency Band Applications," *2019 6th International Conference on Signal Processing and Integrated Networks (SPIN)*, Noida, India, 2019, pp. 87-90.
- [31] G. Amruta and R. Kumar, "Enhancing the Performance Characteristic of Patch Antenna using Split-Ring Resonator Metamaterial," *2020 International Conference on Computational Performance Evaluation (ComPE)*, Shillong, India, 2020, pp. 367-370.
- [32] Y. M. Huang, Y. Zhou, H. Jin, G. Wang and M. Bozzi, "Miniaturized Evanescent Mode Substrate Integrated Waveguide Filter with Mixed-Coupled Folded Complementary Split-Ring Resonators," *2019 IEEE MTT-S International Wireless Symposium (IWS)*, Guangzhou, China, 2019, pp. 1-4.
- [33] M. Gupta, "Conformal Microstrip Filter Design Using Complementary Split Ring Resonator," *2018 4th International Conference on Computing Communication and Automation (ICCCA)*, Greater Noida, India, 2018, pp. 1-4.
- [34] A. Singh, A. Raj, A. Gupta, A. Tiwari and P. Kumar, "Split ring resonator biosensor-an innovative design and analysis," *2020 IEEE 8th International Conference on Photonics (ICP)*, Kota Bharu, Malaysia, 2020, pp. 117-118.
- [35] K. S. Umadevi, S. K. Simon, S. P. Chakyar, J. Andrews and V. P. Joseph, "Wide Band Microwave Absorber using Flexible Broadside Coupled Split Ring Resonator Metamaterial Structure," *2019 Thirteenth International Congress on Artificial Materials for Novel Wave Phenomena (Metamaterials)*, Rome, Italy, 2019, pp. X-453-X-455.
- [36] W. Shahzad, W. D. Hu, A. Samad and L. P. Ligthart, "Complementary Split Ring Resonator based Metamaterial sensor for Dielectric Materials Measurements," *2020 17th International Bhurban Conference on Applied Sciences and Technology (IBCAST)*, Islamabad, Pakistan, 2020, pp. 695-698.
- [37] A. K. Gorur, "A Dual-Band Balun BPF Using Codirectional Split Ring Resonators," in *IEEE Microwave and Wireless Components Letters*, vol. 30, no. 10, pp. 949-952, 2020.

- [38] Y. -R. Ho and C. -L. Yang, "A Wearable Throat Vibration Microwave Sensor Based on Split-Ring Resonator for Harmonics Detection," *2020 IEEE/MTT-S International Microwave Symposium (IMS)*, Los Angeles, CA, USA, 2020, pp. 504-507.
- [39] M. Baghelani, N. Hosseini and M. Daneshmand, "Selective Measurement of Water Content in Multivariable Biofuel Using Microstrip Split Ring Resonators," *2020 IEEE/MTT-S International Microwave Symposium (IMS)*, Los Angeles, CA, USA, 2020, pp. 225-228.
- [40] I. Topaloglu and O. Gurdal, "A second order sensitivity analysis based numerical approach developed for dimension optimization, in electric machine design by electromagnetic design software," *Journal of the Faculty of Engineering and Architecture of Gazi University*, 2010, pp. 363-369.
- [41] F. Korkmaz and I. Topaloglu, "Simulink model of vector controlled linear induction motor with end effect for electromagnetic launcher system," *Elektronika ir Elektrotechnika*, 2014, pp. 29-32.
- [42] M. Hesham and S. O. Abdellatif, "Compact Bandpass Filter Based on Split Ring Resonators," *2019 International Conference on Innovative Trends in Computer Engineering (ITCE)*, Aswan, Egypt, 2019, pp. 301-303.
- [43] H. Kahraman , "Rulet Elektromanyetik Alan Optimizasyon (R-EFO) Algoritması", *Düzce Üniversitesi Bilim ve Teknoloji Dergisi*, vol. 8, no. 1, pp. 69-80, 2020.
- [44] F. Katırcıoğlu ve U. Güvenç , "Sequentially Modified Gravitational Search Algorithm for Image Enhancement", *Düzce Üniversitesi Bilim ve Teknoloji Dergisi*, vol. 8, no. 4, pp. 2266-2288, 2020.